HHS Public Access

Author manuscript

Nat Chem Biol. Author manuscript; available in PMC 2017 May 01.

Published in final edited form as:

Nat Chem Biol. 2016 May ; 12(5): 345–352. doi:10.1038/nchembio.2047.

Malic enzyme tracers reveal hypoxia-induced switch in adipocyte NADPH pathway usage

Ling Liu[1,2,5], **Supriya Shah**[4,5], **Jing Fan**[1,2], **Junyoung O Park**[1,3], **Kathryn E Wellen**[4,5], and **Joshua D Rabinowitz**[1,2,5,*]

[1]Lewis-Sigler Institute for Integrative Genomics, Princeton University, Princeton, New Jersey, USA

[2]Department of Chemistry, Princeton University, Princeton, New Jersey, USA

[3]Department of Chemical and Biological Engineering, Princeton University, Princeton, New Jersey, USA

[4]Department of Cancer Biology, University of Pennsylvania, Philadelphia, Pennsylvania, USA

[5]Diabetes Research Center, University of Pennsylvania, Philadelphia, Pennsylvania, USA

Abstract

The critical cellular hydride donor NADPH is produced through various means, including the oxidative pentose phosphate pathway (oxPPP), folate metabolism and malic enzyme. In growing cells, it is efficient to produce NADPH via the oxPPP and folate metabolism, which also make nucleotide precursors. In nonproliferating adipocytes, a metabolic cycle involving malic enzyme holds the potential to make both NADPH and two-carbon units for fat synthesis. Recently developed deuterium (^{2}H) tracer methods have enabled direct measurement of NADPH production by the oxPPP and folate metabolism. Here we enable tracking of NADPH production by malic enzyme with [2,2,3,3-^{2}H]dimethyl-succinate and [4-^{2}H]glucose. Using these tracers, we show that most NADPH in differentiating 3T3-L1 mouse adipocytes is made by malic enzyme. The associated metabolic cycle is disrupted by hypoxia, which switches the main adipocyte NADPH source to the oxPPP. Thus, ^{2}H-labeled tracers enable dissection of NADPH production routes across cell types and environmental conditions.

NADPH is a key cofactor involved in antioxidant defense and reductive biosynthesis[1]. It can be produced in cells by several enzymes, including glucose-6-phosphate dehydrogenase (G6PDH) and 6-phosphogluconate dehydrogenase in the oxPPP, methylenetetrahydrofolate dehydrogenase (MTHFD) and aldehyde dehydrogenases (ALDHs) in folate metabolism, and

*Correspondence and requests for materials should be addressed to J.D.R. ; Email: joshr@princeton.edu

Author contributions

J.D.R., K.E.W., L.L. and J.F. conceived the project. L.L. performed and analyzed most experiments. L.L., J.O.P., J.F. and J.D.R. conducted the flux analysis. S.S. performed electroporation experiments and analyzed the data. J.D.R. and L.L. wrote the manuscript.

Competing financial interests

The authors declare no competing financial interests.

Additional Information

Any supplementary information, chemical compound information and source data are available in the online version of the paper.

isocitrate dehydrogenases (IDHs) and malic enzyme associated with the tricarboxylic acid (TCA) cycle. The oxPPP is localized to the cytosol and is NADPH specific, whereas different isozymes of MTHFD, ALDH, malic enzyme and IDH are found in the cytosol and mitochondria and may generate NADPH or NADH[2,3]. The importance of the oxPPP in NADPH production is the best established. G6PDH deficiency is the most common human enzyme deficiency and leads to oxidative stress in red blood cells[4].

^{13}C-labeled tracers have long been used to follow metabolic activity, but they provide only indirect information on the sources of redox cofactors such as NADPH. They are inadequate when the same carbon transformation can produce NADPH or NADH depending on the isozyme involved. To address this limitation, hydride transfer from [^{2}H]glucose or [^{2}H]serine into NADPH in cells has been tracked directly by mass spectrometry[5]. Related work has traced compartment-specific NADPH hydride ^{2}H labeling using 2-hydroxyglutarate as a reporter metabolite[6]. 2-hydroxyglutarate is made by NADPH-driven α-ketoglutarate reduction by mutant IDH, with IDH1 localized into the cytosol and IDH2 to mitochondria. Both the direct NADPH ^{2}H labeling measurements and the 2-hydroxyglutarate reporter approach revealed that the oxPPP is the largest cytosolic NADPH source in typical transformed cells in culture, with other pathways collectively making a roughly comparable contribution. Whether different enzymes have a predominant role in certain cell types or conditions remains unknown.

The most NADPH-demanding biosynthetic activity in mammals is fat synthesis, which consumes a majority of cytosolic NADPH in typical transformed cells in culture[5]. In intact mammals, fat synthesis is thought to be localized primarily to liver and adipose tissue[7]. Significant malic enzyme activity was described in adipose tissue more than 50 years ago[8,9]. During adipocyte differentiation, there is coordinate upregulation of ATP citrate lyase and cytosolic malic enzyme (ME1), which together with cytosolic malate dehydrogenase and at the expense of 1 ATP molecule, can convert citrate and NADH into acetyl-CoA, NADPH and pyruvate[10]. Acetyl-CoA and NADPH are the two key substrates for fat synthesis, and the resulting pyruvate can be used to make more citrate. Thus, it is efficient to use malic enzyme to make NADPH in adipose tissue. The quantitative contribution of different NADPH-producing enzymes in adipose, however, remains ill defined. Prior quantitative studies suggest a ~60% contribution from the oxPPP and the remainder from other pathways[11–14].

Here we employ ^{2}H tracing to quantitatively analyze NADPH metabolism in the common tissue culture model of adipose, 3T3-L1 adipocytes. ^{2}H tracers for the oxPPP and folate metabolism were recently established[5,6], but suitable tracers for malic enzyme were lacking. We demonstrate the utility of both [2,2,3,3-^{2}H]dimethyl-succinate and [4-^{2}H]glucose for tracing hydride flux from malate to NADPH and into fat. Combining this approach with ^{13}C labeling studies shows that malic enzyme is the main NADPH source in normoxic 3T3-L1 adipocytes, with total NADPH production more than double that from the oxPPP. Adipocyte differentiation and associated fat synthesis continue in hypoxia, but the mode of NADPH production changes dramatically, with malic enzyme's contribution becoming minimal and the oxPPP's predominant.

RESULTS

Quantitative analysis of 3T3-L1 cell NADPH consumption

3T3-L1 preadipocytes cells grow in standard tissue culture medium and can be induced to differentiate into adipocytes by addition of a hormone cocktail[15,16]. We monitored cell proliferation, cell volume expansion and associated lipid accumulation during the differentiation process (Fig. 1a,b). As we observed the fastest lipid accumulation between days 4 and 7 of differentiation, we used adipocytes at day 5 of differentiation in subsequent analyses of metabolic activity.

NADPH drives the synthesis of deoxyribonucleotides, proline and fatty acids. We investigated NADPH biosynthetic consumption flux in proliferating and differentiating 3T3-L1 cells. To determine the amount of NADPH consumed by deoxyribonucleotide synthesis, we measured the rate of change in cell number and assumed a constant amount of DNA per cell, with 1.25 NADPH per nucleoside (2 per thymidine and 1 per each of the other deoxyribonucleosides). For proline, we measured the rate of protein accumulation and corrected for the average frequency of proline, with 1.5 NADPH per proline[5]. The NADPH consumption by DNA and proline synthesis was, as we expected, greater in proliferating than in differentiating cells (Fig. 1c).

For lipid synthesis, we corrected the observed rate of total cellular fatty acid accumulation for the fraction of fatty acid synthesized *de novo*, which we determined by feeding [U-^{13}C]glucose and [U-^{13}C]glutamine and measuring the extent of fatty acid labeling by mass spectrometry (Supplementary Results, Supplementary Fig. 1). In the proliferating 3T3-L1 cells, fatty acids were assimilated to support growth, but ^{13}C labeling was minimal, indicating fatty acid acquisition primarily by uptake from the medium. In contrast, upon differentiation, fatty acid content per cell increased and was driven by *de novo* synthesis. In proliferating and differentiating cells, the incorporation rate of two-carbon units into fatty acids was 0.011 and 0.120 μmol per day per million cells, respectively, with two NADPH required per two-carbon unit. The fat synthesis rate of the differentiating adipocytes was similar to that observed previously in transformed and cancer cells[5]. Thus, total biosynthetic NADPH consumption in proliferating preadipocytes was relatively low and directed substantially toward deoxyribonucleotide and proline synthesis, whereas in differentiating adipocytes it was higher (similar to that in growing transformed cells) and devoted almost solely to fat synthesis (Fig. 1c).

oxPPP flux and total NADPH generation

We used two complementary methods to measure oxPPP activity. First, we cultured cells in the presence of [1-^{14}C]glucose or [6-^{14}C]glucose and detected the released $^{14}CO_2$. The oxPPP releases C1 of glucose as CO_2. The [6-^{14}C]glucose corrects for release of C1 by other pathways, because C1 and C6 are rendered identical by the triose phosphate isomerase step in glycolysis (Fig. 2a). We determined an oxPPP flux of 0.017 and 0.020 μmol per day per million cells in proliferating and differentiating cells, respectively (Fig. 2b), and confirmed the rate in differentiating cells with [1,2-^{13}C]glucose tracer (Supplementary Fig. 2a–c); these rates are substantially below that previously reported in transformed growing

cells[5]. Next, we fed cells [1-^{2}H]glucose and [3-^{2}H]glucose, which label NADPH in the first (G6PDH) and third step (6-phosphogluconate dehydrogenase) of the oxPPP, respectively[5]. In the proliferating cells, the M+1 fraction of NADPH exceeded that of $NADP^+$ by ~13% (Fig. 2c). Similar NADPH labeling results have been reported in several transformed growing cell lines[5,6]. In contrast, in the differentiating adipocytes, there was much less NADPH labeling from [1-^{2}H]glucose. Thus, in contrast to growing cells, differentiating 3T3-L1 cells derive a substantially smaller fraction of NADPH from the oxPPP.

The [^{2}H]glucose labeling results can be used to quantify the fractional contribution of the oxPPP to total cytosolic NADPH production. The inferred fractional contribution of the oxPPP to NADPH production can be used to deduce the total cytosolic NADPH production rate, which is equal to the absolute oxPPP flux divided by the fractional contribution of the oxPPP to NADPH production[5]

$$f\,\mathrm{NADPH\ from\ oxPPP} = 2 \times (f\mathrm{CO_2\ from\ glucose\ C1} - f\mathrm{CO_2\ from\ glucose\ C6}) \quad (1)$$

$$f\,\mathrm{NADPH\ from\ oxPPP} = 2 \times \frac{\mathrm{NADP^2H}}{\mathrm{NADPH_{total}}} \times \frac{\mathrm{G6P_{total}}}{[^2\mathrm{H}]\mathrm{G6P}} \times f\,\mathrm{NADPH\ from\ all\ cytosolic\ sources} \times \mathrm{C_{KIE}} \quad (2)$$

In equation (1), fCO$_2$ from glucose C1 is based on the measured release rates of [^{14}C]CO$_2$ corrected for the fractional radioactive labeling of glucose (and similarly for C6; Online Methods) and multiplied by two to account for the oxPPP stoichiometry of 2 NADPH per 1 glucose. In equation (2), the measured fractional ^{2}H labeling of NADPH is corrected for the ^{2}H labeling of glucose-6-phosphate (G6P) (Supplementary Fig. 2d) and for the deuterium kinetic isotope effect (C_{KIE})[17] and multiplied by two, as only one of the two hydrogens that are transferred to NADPH via the oxPPP is labeled. Combining equations (1) and (2), the measured absolute oxPPP NADPH production (fNADPH from oxPPP, 0.034 and 0.040 μmol per day per million cells, in proliferating and differentiating cells, respectively) divided by the fractional contribution of the oxPPP (46% and 16%, in proliferating and differentiating cells, respectively) gave a total cytosolic NADPH production flux of approximately 0.074 and 0.250 μmol per day per million cells in proliferating and differentiating cells, respectively. This total NADPH production flux was nearly identical to the independently measured biosynthetic NADPH consumption flux (Fig. 2d). Thus, most NADPH in both proliferating and differentiating cultured cells is consumed for biosynthesis, and mainly for fat synthesis in differentiating cells.

NADPH contribution of folate metabolism

The folate metabolic enzymes MTHFD and ALDH have NADPH-producing dehydrogenase activity. MTHFD is required for oxidizing methylene-THF into the key one-carbon donor formyl-tetrahydrofolate (formyl-THF). In contrast, ALDH does not produce a useful one-carbon donor, but instead oxidizes formyl-THF into THF, CO_2 and NADPH (Fig. 3a).

Cytosolic formyl-THF, which is required by proliferating cells for purine synthesis, can be produced from methylene-THF by the cytosolic methylene-THF dehydrogenase MTHFD1 with concomitant cytosolic NADPH production. Alternatively, it can be made from formate

exported by mitochondria, in which case methylene-THF oxidation occurs in the mitochondria with associated production by MTHFD2 of mitochondrial NADH and (to a lesser extent) NADPH[2,18]. To determine where one-carbon units are made in proliferating 3T3-L1 cells, we fed cells [2,3,3-^{2}H]serine and looked for production of ^{2}H-labeled thymidine triphosphate (TTP). The cytosolic pathway produced doubly labeled TTP, whereas one deuterium was lost in the mitochondrial pathway resulting in single TTP labeling (Supplementary Fig. 2e). We observed only M+1 TTP, indicating minimal cytosolic MTHFD1 flux in the direction of NADPH production (Supplementary Fig. 2f).

Given these results, we focused on the complete oxidation of one-carbon units by the combined action of MTHFD and ALDH, which can be traced on the basis of release of CO_2 from [3-^{14}C]serine and [2-^{14}C]glycine. We observed substantial release of serine C3 as CO_2, indicating that the complete one-carbon oxidation pathway is actively producing NADPH (Fig. 3b). The absolute flux of NADPH produced by folate metabolism, however, was smaller than the oxPPP flux. Consistent with the methylene-THF oxidation pathway resulting in a modest contribution to total NADPH production, feeding of [2,3,3-^{2}H]serine, the main pathway substrate, resulted in ~3% labeling of NADPH at its redox-active hydride (Supplementary Fig. 2g). Thus, in differentiating 3T3-L1 adipocytes, folate metabolism contributes modestly to NADPH production.

Tracing carbon flux through malic enzyme

The above analysis implies that a majority of NADPH in differentiating adipocytes comes from sources other than the oxPPP and folate metabolism (Fig. 3c). We accordingly considered malic enzyme. To evaluate total malic enzyme flux (f_{ME}), we analyzed cells fed [U-^{13}C]glutamine, whose metabolism through the TCA cycle and malic enzyme labels pyruvate (Online Methods and Supplementary Fig. 3). Assuming that pyruvate and malate are labeled similarly in both mitochondria and cytosol we can use the equation

$$\frac{f_{\mathrm{ME}}}{f_{\mathrm{glycolysis}}}=\frac{\mathrm{Pyr}_{\mathrm{M+3}}}{\mathrm{Pyr}_{\mathrm{M+0}}}\times\frac{\mathrm{Mal}_{\mathrm{total}}}{\mathrm{Mal}_{\mathrm{M+4}}+0.5\times\mathrm{Mal}_{\mathrm{M+3}}} \quad (3)$$

This assay measures gross flux from malate (mal) to pyruvate (pyr), which will exceed the net malic enzyme flux when alternative pathways between malate and pyruvate are active (for example, gluconeogenesis, reverse pyruvate carboxylase or reverse malic enzyme[9,19–21]). It also does not account for pyruvate and malate compartmentation or identify whether malic enzyme is making NADH or NADPH.

Similarly to many transformed cell lines, proliferating 3T3-L1 cells showed only trace pyruvate labeling from glutamine[22] (Fig. 4a). Upon differentiation, however, there was extensive labeling, with malate-to-pyruvate flux producing ~15% of the pyruvate pool (Fig. 4b). Owing to the speed of glycolysis (glucose uptake rate = 6.4 μmol per day per million cells), total gross flux from malate to pyruvate on day 5 was 2.4 μmol per day per million cells, approximately ten-fold the measured total NADPH consumption and production rates.

To evaluate whether gluconeogenic flux involving the combined action of malate dehydrogenase, phosphoenolpyruvate carboxykinase (PEPCK) and pyruvate kinase contributes to the observed pyruvate labeling, we monitored the labeling of phosphoenolpyruvate (PEP), the direct product of PEPCK, and the more abundant phosphoglycerate (adjacent in glycoylsis), by [U-^{13}C]glutamine. We observed only trace labeling, thereby ruling out a major contribution of the gluconeogenic pathway (Fig. 4c).

We next explored whether quantitative metabolic flux analysis (MFA) of ^{13}C-labeling data for the full set of measurable central carbon metabolites would be sufficient to determine net malic enzyme flux and its compartmentation. Specifically, we developed a carbon-and redox-balanced flux model of central metabolism and searched computationally for flux values that fit experimental data for nutrient uptake, waste excretion and metabolite ^{13}C-labeling data in cells fed [U-^{13}C]glucose or [U-^{13}C]glutamine (Fig. 4d and Supplementary Table 1). For simplicity, we allowed only forward flux through pyruvate carboxylase and malic enzyme. A minimal reaction network with only cytosolic malic enzyme (ME1) did not fit the data as well as the network including also mitochondrial malic enzyme or pyruvate carboxylase reversibility (Supplementary Table 2 and Supplementary Fig. 4). In the case with ME1 only (Fig. 4d), malic enzyme flux was ~2.9 μmol per day per million cells. Inclusion of mitochondrial malic enzyme (Fig. 4d) did not significantly change the total malic enzyme flux but rendered the ME1 flux indeterminant (confidence interval 0.2 to 2.0 μmol per day per million cells) (Supplementary Table 2). Thus, ^{13}C tracers were insufficient to determine cytosolic malic enzyme activity and associated NADPH production.

[2,2,3,3-^{2}H]dimethyl succinate tracer for malic enzyme

We next sought to track hydride transfer mediated by malic enzyme. Previous efforts to trace such activity with [2,3,3,4,4-^{2}H]glutamine were unsuccessful[5] and were similarly unsuccessful here owing to loss of the ^{2}H label throughout the intervening TCA cycle reactions (Supplementary Fig. 5a). As an alternative, we fed cells the membrane-permeable succinate analog [2,2,3,3-^{2}H]dimethyl succinate (Supplementary Fig. 5a,b). Tracer addition increased the cellular concentration of succinate without markedly perturbing other metabolite concentrations or flux (Supplementary Fig. 6). We followed labeling from [2,2,3,3-^{2}H]dimethyl succinate through the C2 hydride of malate to NADPH and then to newly synthesized fatty acids (Fig. 5a). NADPH labeling at its redox-active hydride was analyzed by comparing the M+1 fraction of NADPH to that of NADP^{+}. In the absence of [2,2,3,3-^{2}H]dimethyl succinate, the NADP^{+} and NADPH labeling patterns were identical (Supplementary Fig. 5b). Addition of tracer resulted in increased labeling of NADPH but not NADP^{+} in differentiating 3T3-L1 cells, with 3.4% ± 0.3% (mean ± s.d.) of the total adipocyte NADPH labeled (Fig. 5b). Analysis of fatty acids, which reflects cytosolic NADPH specifically and thus ME1, similarly revealed selective ^{2}H labeling in differentiating adipocytes (Fig. 5c). Quantitative analysis of the mass isotope distribution of a set of abundant fatty acids (omitting pre-existing fatty acids and those acquired by uptake from the medium, as determined by ^{13}C labeling) revealed an average hydride ^{2}H-labeling fraction of 2.87% ± 0.31% (Supplementary Fig. 7). Adjustment for the kinetic isotope effect in hydride transfer from NADPH to fat (~1.1)[23] yielded an associated cytosolic NADPH

labeling fraction of 3.2% ± 0.5%, in agreement with the directly measured whole-cell NADPH labeling.

Converting the NADPH labeling fraction from [2,2,3,3-^{2}H]dimethyl succinate into the fractional NADPH contribution of malic enzyme requires correction for (i) fractional ^{2}H labeling of cytosolic malate's C2 hydride and (ii) the malic enzyme deuterium kinetic isotope effect (~1.5, Online Methods).

$$f_{\text{NADPH from ME1}} = \frac{\text{NADP}^2\text{H}}{\text{NADPH}} \times \frac{\text{Mal}}{\text{Mal}_{\text{C2-deuteron}}} \times f_{\text{NADPH from all sources}} \times \text{C}_{\text{KIE}} \quad (4)$$

Forward flux from [2,2,3,3-^{2}H]succinate results in [2,3-^{2}H]malate, i.e., M+2 malate (Supplementary Fig. 8a). The observed fraction of M+2 malate was, however, only 1.5%. The larger peak was M+1 malate (Supplementary Fig. 8b). Reverse flux through malate dehydrogenase can produce M+1 malate labeled at the C3 hydride ([3-^{2}H]malate). As fumarate is symmetric, fumarase interconverts [3-^{2}H] and [2-^{2}H]malate (Supplementary Fig. 8a). Because malic enzyme produces NADP^{2}H selectively from malate labeled at the C2 hydride, it was critical to determine the relative abundance of [2-^{2}H]malate and [3-^{2}H]malate. [3-^{2}H]malate (and also [2,3-^{2}H]malate) yields M+1 oxaloacetate and aspartate, whereas [2-^{2}H]malate yields unlabeled oxaloacetate and aspartate. Hence, subtracting the fraction of M+1 aspartate from the sum of M+1 and M+2 malate gives the fraction of [2-^{2}H]malate, which was ~6.4%. The sum of [2-^{2}H]malate and [2,3-^{2}H]malate, which is the fraction of malate that is capable of making NADP^{2}H, was 7.9% (Fig. 5d and Online Methods). Thus, although [2,2,3,3-^{2}H]dimethyl succinate labeled only ~3.2% of NADPH, the fraction of NADPH generated via malic enzyme was ~60%.

[4-^{2}H]glucose as a malic enzyme tracer

Dimethyl succinate is not a typical circulating nutrient. Conversion of [2,2,3,3-^{2}H]dimethyl succinate to [2-^{2}H]malate requires oxidation of succinate to fumarate by succinate dehydrogenase (complex II) in the inner mitochondrial membrane, and the resulting labeled malate must traffic to the cytosol to feed ME1. Incomplete mixing between the mitochondria and cytosol could result in overestimation of cytosolic malate labeling and thus underestimation of ME1's contribution to NADPH. We accordingly sought an alternative tracer strategy involving only standard nutrients, where labeled malate would be made directly in the cytosol.

One way to generate cytosolic [2-^{2}H]malate is via malate dehydrogenase-catalyzed reduction of oxaloacetate by NAD^{2}H. [4-^{2}H]glucose can label cytosolic NADH via glyceraldehyde-3-phosphate dehydrogenase[6] (Fig. 5e). Compared to the dimethyl succinate tracer, [4-^{2}H]glucose resulted in a similar extent of [2-^{2}H]malate labeling (Supplementary Fig. 8c). We observed small and similar amounts of labeling of NADP$^+$ or NADPH by [4-^{2}H]glucose in the proliferating cells, indicating incorporation of ^{2}H-labeled ribose into newly synthesized NADP$^+$ without redox-active hydride labeling (Fig. 5f). In contrast, we observed preferential labeling of NADPH over NADP$^+$ in the differentiating adipocytes, indicating flux into NADPH's redox-active hydride via malic enzyme. Consistent with this,

[4-^{2}H]glucose labeled fatty acids selectively in the differentiating cells (Fig. 5g). Quantitatively, the extent of redox-active NADPH hydride labeling was identical (within error) for both the [4-^{2}H]glucose and the dimethyl succinate tracers (Fig. 5h).

We integrated the ME1 flux constraint from the ^{2}H tracers with the nutrient uptake, waste excretion and ^{13}C-tracer data via quantitative metabolic flux analysis of the network, including ME1 and mitochondrial malic enzyme, and this resulted in a coherent set of whole-cell flux values (Fig. 4d). In the absence of pyruvate carboxylase or malic enzyme reversibility, all flux values were well defined. Inclusion of such reversibility rendered mitochondrial flux indeterminant without affecting the fit or affecting ME1 flux (Supplementary Table 2). The confidence interval for NADPH production rate was 0.4–0.8% of the glucose uptake rate for the oxPPP and 2.7–3.5% for ME1 (Supplementary Table 1).

Genetic confirmation of ME1's NADPH contribution

Both ME1 and NADH-producing mitochondrial malic enzyme 2 (ME2) have been shown through small hairpin RNA–mediated knockdown to be required for adipocyte differentiation[24]. We observed that ME1 protein, but not ME2 or ME3 protein, increased greatly during adipocyte differentiation (Supplementary Fig. 9a). To evaluate the functional significance of ME1 relative to other cytosolic NADPH-producing enzymes, we used short interfering RNA (siRNA) to knock down, on differentiation day 2, G6PDH (the committed enzyme of the oxPPP), MTHFD1 (required for cytosolic one-carbon unit oxidation), IDH1 (the cytosolic NADPH-generating isocitrate dehydrogenase) and ME1 (Fig. 5i and Supplementary Fig. 9b). Knockdown of ME1, but not the other enzymes, decreased fatty acid accumulation in the differentiating adipocytes (Fig. 5j). Moreover, ME1 knockdown decreased carbon flux from malic acid to pyruvate (Supplementary Fig. 9c–e) and fatty acid labeling from [2,2,3,3-^{2}H]dimethyl succinate (Fig. 5k). Thus, ME1 is the main source of NADPH driving fatty acid synthesis in normoxic adipocytes and is required for effective lipogenesis.

Impact of hypoxia on adipocyte metabolism

Quantitative flux analysis in the differentiating adipocytes revealed a metabolic cycle in which pyruvate is generated by malic enzyme and consumed by pyruvate carboxylase[25] and pyruvate dehydrogenase. This cycle is efficient in terms of minimizing the transport of substrates between the cytosol and mitochondrion (Supplementary Fig. 9f). We were curious about whether malic enzyme would continue to be the predominant NADPH source under conditions in which the cycle is disrupted, such as by inhibition of pyruvate dehydrogenase activity in hypoxia[26,27]. Understanding the impact of hypoxia on differentiating adipocyte metabolism is also of potential medical relevance, as obesity has been proposed to result in hypoxia in adipose tissue[28,29].

We began by determining whether differentiation would proceed in 1% oxygen. Though attenuated, fatty acid synthesis, associated lipid accumulation and adipocyte markers were induced by differentiation in hypoxia (Supplementary Fig. 10a–e). The source of the fatty acid carbon changed from mainly glucose to mainly glutamine, as also occurs in hypoxic cancer cells[30,31], with increased glucose uptake and lactate excretion (Supplementary Fig.

10f,g). To evaluate NADPH production routes in hypoxic differentiating adipocytes, we traced hydride labeling into fat from [1-^{2}H]glucose and [3-^{2}H]glucose to probe the oxPPP and [2,2,3,3-^{2}H]dimethyl succinate and [4-^{2}H]glucose to probe malic enzyme. Hypoxia resulted in markedly increased labeling from both oxPPP tracers (Fig. 6a and Supplementary Fig. 11a–e) and near-complete elimination of labeling from both malic enzyme tracers (Fig. 6b and Supplementary Fig. 11f). After correcting for substrate labeling and the deuterium kinetic isotope effect[17,32,33] we found that the contribution of the oxPPP increased from 21% ± 4% in normoxia to 55% ± 5% in hypoxia, whereas the contribution of malic enzyme decreased from 60% ± 5% to 3% ± 2% (mean ± s.d., n = 3). Thus, in response to hypoxia, the main lipogenic NADPH source switched from malic enzyme to the oxPPP (Fig. 6c,d). We also compared hypoxia starting at day 0 of differentiation to hypoxia initiated midway through the differentiation process (starting at day 3). The ‘switch’ into hypoxia produced an intermediate phenotype in terms of contributions from NADPH production routes (Supplementary Fig. 12). To investigate the mechanism by which NADPH production was being controlled, we measured protein levels of ME1 and G6PDH. The oxPPP protein level did not change markedly in response to hypoxia, but ME1 decreased (Supplementary Fig. 10e). Together, these data reveal that differentiation in hypoxia shifts the main 3T3-L1 adipocyte NADPH production route to the oxPPP, in part by suppressing ME1 enzyme abundance.

DISCUSSION

Cells use two fundamental energy currencies: high-energy phosphate bonds and high-energy electrons. High-energy phosphate bonds in the form of ATP are produced in significant quantities by only two routes—glycolysis and oxidative phosphorylation—with glycolysis a significant ATP source specifically when oxygen is limited. High-energy electrons in the form of NADPH, in contrast, can be produced by a variety of pathways. The physiological rationale for use of one pathway rather than another remains unclear. Published studies have used ^{2}H tracers to quantitatively examine NADPH production pathways in transformed growing cells[5,6]. These analyses led to two major conclusions: (i) most cytosolic NADPH in growing cells is used for reductive biosynthesis, not antioxidant defense, and (ii) the largest NADPH contributor is the oxPPP, and folate metabolism also has a role. Growing cells have a high demand for nucleotide synthesis, which requires precursors generated by the oxPPP and folate metabolism. The oxPPP and folate flux observed in growing cells are necessary for meeting ribose phosphate and 10-formyl-THF demand and can also provide most of the required NADPH[5]. Thus, it is physiologically efficient for growing cells to use the oxPPP and/or folate metabolism for NADPH production.

Here we examine NADPH metabolism in 3T3-L1 cells, which stop growing but remain biosynthetically active on differentiation. We show that both total biosynthetic NADPH demand and NADPH production increase, upon differentiation, to a level comparable to that in typical transformed cells. The overall metabolic requirements of differentiating adipocytes are, however, distinct. Differentiating adipocytes do not engage in significant nucleotide synthesis and thus have minimal need for ribose phosphate and 10-formyl-THF. The fractional NADPH contribution of these pathways drops. Instead, in normoxic differentiating adipocytes, most NADPH is made by malic enzyme. We confirmed this using a combination

of classical [^{13}C]glutamine tracing into pyruvate augmented by more global flux analysis and a newly developed method for directly tracing NADP^{2}H production by malic enzyme.

Despite significant interest in malic enzyme's role in cancer[13] and obesity[34–36], previous methods did not allow direct following of NADPH production from malic enzyme in cells. Carbon isotope tracer studies, although valuable[22,25], cannot directly differentiate NADH- and NADPH-dependent malic enzyme. Although recent work observed NADH and NADPH labeling from [4-^{2}H]glucose, the NADPH labeling was attributed to an unknown mechanism rather than malic enzyme. The two tracers that we provide here, [2,2,3,3-^{2}H]dimethyl succinate and [4-^{2}H]glucose, both produce [2-^{2}H]malate, which in turn makes NADP^{2}H and ^{2}H-labeled fatty acids. Production of labeled malate by [2,2,3,3-^{2}H]dimethyl succinate is more direct but relies on a nonphysiologic uptake mechanism and transfer of malate from mitochondrion to cytosol. Accordingly, [4-^{2}H]glucose may be more generally applicable, as it uses a physiological uptake mechanism and sequence of cytosolic reactions to label malate and is better suited to potential future *in vivo* application.

An important virtue of using two tracers is that any one method may be subject to nonrandom error (for example, due to hydrogen-deuterium exchange, compartmentation or factors affecting the kinetic isotope effect). Some such errors may be common to both tracers, which feed through [2-^{2}H]malate. Moreover, each tracer labels metabolites in addition to malate, which can potentially result in ^{2}H labeling of NADPH or fatty acids through other routes. For example, turning of the TCA cycle converts [3-^{2}H]malate into [^{2}H]isocitrate labeled at the hydride transferred to NADPH by IDH1 and IDH2. Although we did not observe significant (iso)citrate labeling from these tracers in adipocytes, we did in some other cell types. These observations highlight the need for careful consideration of all possible means of gaining or losing ^{2}H labeling when such tracers are used. That said, our main findings appear to be robust. Both tracers gave quantitatively indistinguishable results: a malic enzyme contribution to cytosolic NADPH of roughly 60% in normoxia and 3% in hypoxia.

Among the multitude of possible NADPH production routes, why do normoxic adipocytes rely on malic enzyme? And why does this change in hypoxia? Fatty acid synthesis requires cytosolic acetyl-CoA. Pyruvate is converted to acetyl-CoA selectively in the mitochondrion. This acetyl-CoA is carried into the cytosol as citrate, which is then re-converted into oxaloacetate and acetyl-CoA in the cytosol by ATP-citrate lyase[37]. Reduction of oxaloacetate by cytosolic malate dehydrogenase yields cytosolic malate. Conversion of this malate into pyruvate and NADPH by malic enzyme regenerates pyruvate. This cycle[38] serves dual purposes in adipocytes: (i) production of cytosolic acetyl-CoA and (ii) generation of NADPH from reducing equivalents originally derived from glycolysis as NADH (Supplementary Fig. 9f).

This pyruvate-citrate cycle requires mitochondrial acetyl-CoA made by pyruvate dehydrogenase, an enzyme that is inactivated by multiple mechanisms in hypoxia. Thus, disruption of the pyruvate-citrate cycle, and the associated switch from glucose to glutamine carbon for lipogenesis, is a logical consequence of cultivation in low oxygen. Production of cytosolic acetyl-CoA driven by glucose or glutamine requires ATP-citrate lyase and thus

produces oxalo-acetate, which can undergo NADH-driven reduction to malate. Therefore, use of malic enzyme to make NADPH in hypoxia should be feasible. This makes the shift away from malic enzyme toward the oxPPP yet more notable. Elucidation of the underlying regulatory mechanisms is an objective of future research.

In summary, in both growing and differentiating normoxic adipocytes, NADPH production is carried out by pathways that also have other important physiological roles. In growing cells, the pathways are coupled to nucleotide synthesis; in differentiating adipocytes, the pathways are coupled to generation of cytosolic acetyl-CoA. Hypoxia switches the primary NADPH production route in differentiating adipocytes back to the oxPPP. Much as malic enzyme has a particularly important role in making NADPH in normoxic differentiating adipocytes, we hypothesize that other NADPH-producing enzymes, such as IDH[36], have predominant roles in specific cell types and settings, which remain to be elucidated. Accordingly, the variety of feasible NADPH production pathways can be rationalized as allowing metabolic efficiency across diverse cell types and conditions with distinct total metabolic requirements.

ONLINE METHODS

Cell culture, gene knockdown with siRNA and antibodies

3T3-L1 preadipocytes were obtained from American Type Culture Collection and confirmed to be mycoplasma free by MycoAlert Mycoplasma Detection Kit (Lonza, LT07-218). 3T3-L1 preadipocytes were grown in DMEM (Cellgro, 10-017) with heat-inactivated 10% FBS (Gibco). Adipogenesis was induced in 3T3-L1 preadipocytes with a cocktail containing 5 μg/ml insulin, 0.5 mM isobutylmethylxanthine, 1 μM dexamethasone and 5 μM troglitazone (Sigma-Aldrich). After 2 d, new medium was added and cells were maintained in 5 μg/ml insulin. Cell number was determined with an automatic cell counter (Invitrogen). Packed cell volume was determined with PCV tubes (TPP). Pooled control siRNAs were from Dharmacon (D-001810-10-20). All targeted siRNAs were from Santa Cruz Biotechnology: G6PDH (sc-60668), MTHFD1(sc-61083), IDH1(sc-60830) and ME1 (sc-149342). siRNA were transfected into 3T3-L1 adipocytes on day 2 after differentiation using Lipofectamine RNAiMAX (Invitrogen) and an Amaxa Nucleofector for electroporation. Timeline of knockdown experiments can be found in Supplementary Figure 9b,c. The antibodies to the following proteins were purchased from the indicated sources: ME1 (Abcam, ab97445, 1:1,000 dilution), ME2 (Abcam, ab139686, 1:1,000 dilution), ME3 (Abcam, ab172972, 1:2,000 dilution), G6PDH (Abcam, ab993, 1:1,000 dilution), β-actin (Abcam, ab8229, 1:2,000 dilution), MTHDF1 (Abgent, abin785327, 1:1,000 dilution); IDH1 (Proteintech, 12332-1-AP, 1:2,000 dilution), PPAR-γ (Santa Cruz, sc7196, 1:1,000 dilution) and tubulin (Sigma-Aldrich, T6199, 1:1,000 dilution). Quantitative PCR was performed on purified cDNA samples. Gene expression data were normalized to 18S rRNA. Primers used were SLC2A1(Glut1)-FWD, CCCAGAAGGTTATTGAGGAG; SLC2A1(Glut1)-REV, AGAAGGAACCAATCATGCC; *SLC2A4*(Glut4)-FWD, GCCCGAAAG AGTCTAAAGC; SLC2A4(Glut4)-REV, CTTCCGTTTCTCATCCTTCAG; PPARγ-FWD, TGGCATCTCTGTGTCAACCATG; PPARγ-REV, GCATGGT GCCTTCGCTGA; RETN-FWD, CTGTCCAGTCTATCCTTGCACAC; RETN-REV,

CAGAAGGCACAGCAGTCTTGA; FABP4-FWD, ACAAAATGTGT GATGCCTTTGTGGGAAC; and FABP4-REV, TCCGACTGACTATTGT AGTGTTTGATGCAA.

Isotopic labeling

The following isotopic tracers were purchased from the indicated sources: [2,3,3-^{2}H]serine, [1-^{2}H]glucose, [3-^{2}H]glucose, [U-^{13}C]glutamine and [U-^{13}C]glucose (Cambridge Isotope Laboratories) and [2,2,3,3-^{2}H]dimethyl succinate (Sigma-Aldrich). Isotope-labeled glucose and glutamine medium was prepared from phenol red–, glucose-, glutamine-, sodium pyruvate–, sodium bicarbonate–free DMEM powder (Cellgro) supplemented with 3.7 g/L sodium bicarbonate, 25 mM glucose and 4 mM glutamine. Isotope-labeled serine medium was prepared from scratch following the standard DMEM formula, by mixing together stock solutions containing vitamins, amino acids without serine, inorganic salts, and glucose, and thereafter supplemented with 42 mg/L [2,3,3-^{2}H]serine. Isotope-labeled succinate medium was prepared from DMEM powder, 25 mM glucose, 4 mM glutamine supplemented with 2 mM [2,2,3,3-^{2}H]dimethyl succinate. In HEK293T cells (but not the 3T3-L1 cells studied here) decreasing the glucose and glutamine levels in DMEM to 10 mM and 1 mM, respectively, increases fractional malate labeling from the tracer and thereby facilitates malic enzyme flux measurement. Isotopic medium was supplemented with 10% dialyzed FBS (Sigma-Aldrich) and, for differentiating cells only, 5 μg/ml insulin.

Metabolite measurements

Cells were grown in 6-cm tissue culture dishes, and the labeled medium was replaced every day and 2 h before extracting metabolites. Because labeling of glycolytic and oxPPP intermediates and the redox-active hydride of NADPH reaches steady state over ~5 min where for TCA intermediates this can take several hours[39], we performed oxPPP tracing with [1-^{2}H]glucose and [1,2-^{13}C]glucose for a minimum of 30 min and other labeling experiments for a minimum of 12 h to ensure steady-state labeling. Metabolism was quenched and metabolites were extracted by aspirating medium and immediately adding 2 mL −80 °C 80:20 methanol/water. After 20 min of incubation on dry ice, the resulting mixture was scraped, collected into a centrifuge tube, and centrifuged at 10,000 × *g* for 5 min. Insoluble pellets were re-extracted with 1 mL −80 °C 80:20 methanol/water on dry ice. The supernatants from two rounds of extraction were combined, dried under N_2, resuspended in 1 mL water, and analyzed within 6 h by reversed-phase ion-pairing chromatography coupled with negative-mode ESI high-resolution MS on a stand-alone orbitrap (Thermo)[40]. For lipid extraction, cells were quenched with 2 mL −20 °C 0.1 M HCl in 50:50 methanol/water solution incubated on ice for 20 min. The resulting supernatant was extracted with 1 mL chloroform. The chloroform extract was dried under N_2, saponified with 1 mL 0.3 M KOH in 9:1 methanol/water solution at 80 °C for 1 h and acidified by formic acid. Fatty acids were then subject to two rounds of extraction with 1 mL hexane. The hexane from two rounds of extraction was combined, dried under nitrogen, resuspended in 1 mL 1:1:0.3 chloroform/methanol/water and analyzed by reversed-phase ion-pairing chromatography coupled with negative-mode ESI high-resolution MS on a quadrupole time-of-flight (TOF) mass spectrometer (Agilent Technologies model 6550)[41]. All isotope labeling patterns were corrected for natural ^{13}C abundance.

Quantification of NADPH consumption

NADPH consumption by reductive biosynthesis in the proliferating cells was assessed as described previously[5]. Briefly, we determined experimentally the biomass fraction (normalized to cell number) of DNA (DNA assay kit, Life Technologies), total protein (DC protein assay kit, Bio-Rad), proline (LC/MS), and fatty acids (LC/MS). Then, for each component, we measured the relative contribution of different acquisition routes (for example, biosynthesis versus uptake). The resulting total NADPH consumption is given by:

$$\text{NADPH consumption}=\sum_i \left(\frac{\text{product } i}{\text{cell}}\right)\times\left(\frac{\text{NADPH consumed}}{\text{product } i}\right)\times\text{growth rate} \quad (5)$$

For the differentiating cells, because growth rate is not well defined and biomass composition is changing, we instead inferred DNA synthesis on the basis of rate of increase in cell number (which was negligible by day 5) and measured directly the rate of increase in protein and fat:

$$\text{NADPH consumption}=\sum_i \left(\frac{\text{newly synthesized product } i}{\text{cell}}\right)\times\left(\frac{\text{NADPH consumed}}{\text{product } i}\right) \quad (6)$$

Taking NADPH consumed by fatty acid biosynthesis as an example, we corrected for newly synthesized fatty acid on the basis of ^{13}C enrichment from [U-^{13}C]glucose and [U-^{13}C]glutamine. For each fatty acid species, the unlabeled fraction comes either from pre-existing fat (synthesized or taken up before the labeling began) or from fat taken up directly from serum in the medium; neither of these consume NADPH. Because only the fraction of fatty acid newly synthesized from two-carbon units during the labeling interval uses NADPH, the amount of a newly synthesized fatty acid species (such as palmitate) where labeling fractions are M+0, M+1, and so on, is given by:

$$\text{Newly synthesized palmitate}=\text{palmitate amount}\times\sum_{i=1}^{16}\frac{(M+i)\times i}{16} \quad (7)$$

Malic enzyme (ME) carbon flux

Gross carbon flux from malate to pyruvate, ignoring compartmentation, was quantified on the basis of pyruvate labeling from [U-^{13}C]glutamine. Because the observed fractions of M+1 and M+2 pyruvate were small (their sum is <0.5%) relative to M+3 pyruvate (3%, Supplementary Fig. 3b), the analysis was based solely on the observed M+3 pyruvate signal corrected for the fraction of malate capable of making M+3 pyruvate. Forward flux from [U-^{13}C]glutamine results in M+4 malate ([1,2,3,4-^{13}C]malate, fractional abundance ~20%). Reductive carboxylation of glutamine coupled to citrate lyase can produce M+3 malate (total fractional abundance ~8%) in the form [2,3,4-^{13}C]malate, which produces M+2, not M+3, pyruvate. Malate M+3 exists also as [1,2,3-^{13}C]malate, which produces M+3 pyruvate. Assuming rapid exchange between malate and fumarate (which is symmetric), the

abundances of [1,2,3-^{13}C]malate and [2,3,4-^{13}C]malate will be equal; incomplete exchange will result in less [1,2,3-^{13}C]malate.

$$\frac{f_{\mathrm{ME}}}{f_{\mathrm{glycolysis}}}=\frac{\mathrm{Pyr}_{\mathrm{M+3}}}{\mathrm{Pyr}_{\mathrm{unlabeled}}}\times\frac{\mathrm{Mal}_{\mathrm{total}}}{\mathrm{Mal}_{\mathrm{M+4}}+a\times\mathrm{Mal}_{\mathrm{M+3}}}\left(a=\frac{\mathrm{Mal}_{[1,2,3-^{13}\mathrm{C}]}}{\mathrm{Mal}_{[1,2,3-^{13}\mathrm{C}]}+\mathrm{Mal}_{[2,3,4-^{13}\mathrm{C}]}}\approx 0.5\right) \quad (8)$$

Equation (8) applies when malic enzyme flux is much smaller than glycolytic flux; otherwise, it is necessary to include a term to account for unlabeled pyruvate made via malic enzyme.

CO_2 release and oxPPP flux

$^{14}CO_2$ flux was quantified as previously described[5]. Briefly, cells were grown in 12.5-cm^2 tissue culture flasks with DMEM with low bicarbonate (0.74 g/L) and additional HEPES (6 g/L, pH 7.4). ^{14}C tracer was added to the medium and the flask was sealed with a stopper with a center well (Kimble Chase) containing thick pieces of filter paper saturated with 200 μL 10 M KOH. Cells were incubated for 24 h. Thereafter, 1 mL 3 M acetic acid was added to the culture medium to quench metabolism. Filter paper (and any associated residue) in the center well was collected into a liquid scintillation cocktail (PerkinElmer). The signal was corrected for intracellular substrate labeling according to percentage of radioactive tracer in the medium and the fraction of particular intracellular metabolite from medium uptake, which was measured by ^{13}C tracer. The ^{14}C flux (per cell number per time) after correction is given by:

$$^{14}\mathrm{CO}_2=\frac{\mathrm{C14\ signal}}{\mathrm{tracer\ activity}\times\mathrm{labeling\ time}\times\mathrm{cell\ number}}\times\frac{\mathrm{C12\ substrate}}{\mathrm{C14\ tracer}}\times\frac{\mathrm{fraction\ medium\ nutrient\ C13\ labeled}}{\mathrm{fraction\ intracellular\ substrate\ C13\ labeled}} \quad (9)$$

Nutrient uptake and waste excretion rates

Glucose uptake and lactate excretion were measured by Abcam enzyme assay kits ab65333 and ab65331 and found to be 6.48 and 10.32 μmol per day per million cells, respectively; glycerol excretion was measured by the commercial enzyme assay kit MAK117 (Sigma-Aldrich) to be 0.14 μmol per day per million cells; glutamine and dimethyl succinate uptake and glutamate, alanine, proline and asparagine secretion were measured by LC/MS to be 1.28, 0.32, 0.6, 0.52, 0.088 and 0.08 μmol per day per million cells, respectively; and oxygen consumption was measured by a Seahorse XF Extracellular Flux Analyzer to be 4.76 μmol per day per million cells.

Quantification of fraction NADP^{2}H

The whole-cell fraction of NADPH redox-active hydride labeled (x) was determined from the labeling pattern of NADP$^+$ and NADPH from the same sample incubated with ^{2}H precursors. Let a_0 be the unlabeled fraction of NADP$^+$, a_1 be its M+1 fraction, and so on. We obtained x to best fit the mass isotope distributions vectors (*NADP*$^+$, *NADPH*) by least square fitting in MATLAB:

$$NADP^{+}=\begin{bmatrix} a_0 \\ a_1 \\ a_2 \end{bmatrix} \quad NADPH=\begin{bmatrix} a_0(1-x) \\ a_1(1-x)+a_0x \\ a_2(1-x)+a_1x \\ a_2x \end{bmatrix} \quad (10)$$

Calculation of ME1-dependent NADP^{2}H flux

Converting the whole-cell NADPH labeling fraction from [2,2,3,3-^{2}H]dimethyl succinate into the fractional NADPH contribution of malic enzyme requires correction for (i) ^{2}H labeling of malate's C2 hydride (equation (11)) and (ii) the deuterium kinetic isotope effect of ME1.

$$\frac{\mathrm{Mal}_{\mathrm{C2-deuteron}}}{\mathrm{Mal}}=\frac{[2-^2\mathrm{H}]\mathrm{Mal}}{\mathrm{Mal}}+\frac{[2,3-^2\mathrm{H}]\mathrm{Mal}}{\mathrm{Mal}} = \left(\frac{\mathrm{Mal}_{[M+1]}+\mathrm{Mal}_{[M+2]}}{\mathrm{Mal}}\right)-\left(\frac{\mathrm{Asp}_{[M+1]}}{\mathrm{Asp}}-\frac{\mathrm{Mal}_{[M+2]}}{\mathrm{Mal}}\right) \quad (11)$$

Correction for isotope effect was as previously described[5]:

$$\frac{F_{\mathrm{D}}}{F_{\mathrm{H}}}=\frac{x}{(1-x)}\times\frac{v_{\mathrm{D}}}{v_{\mathrm{H}}} \quad (12)$$

where F_{D} is flux producing NADP^{2}H, F_{H} is flux producing unlabeled NADPH, x is the fraction of [2-^{2}H]malate (7.9% calculated from equation (9)), and $v_{\mathrm{D}}/v_{\mathrm{H}}$ is the kinetic isotope effect for the isolated enzyme, 1.47 ± 0.02 (ref. [42]). Error estimates for the calculated NADPH production fluxes include propagation of the experimental error in the substrate labeling fractions.

Determination of the cytosolic NADPH-labeling fraction on the basis of fatty acid ^{2}H labeling requires correction for (i) the fraction of the individual fatty acids species that is imported rather than synthesized *de novo* and (ii) any ^{2}H labeling that can enter fatty acids via their acetyl groups. In the proliferating condition, cells were maintained at ≤80% confluency (ambient oxygen) with no differentiation reagents. In the differentiating condition, both differentiation cocktail and tracer were added starting on day 0. To correct for the import of fatty acids, the mass isotope distribution vectors for combined [U-^{13}C]glucose and [U-^{13}C]glutamine labeling and separately for [2,2,3,3-^{2}H]dimethyl succinate labeling were corrected for natural ^{13}C abundance. Then, the observed M+0 fraction from the combined [U-^{13}C]glucose and [U-^{13}C]glutamine labeling experiment was subtracted from the M+0 fraction from the [2,2,3,3-^{2}H]dimethyl succinate labeling experiment, as this fraction of fatty acids was not made during the duration of the labeling experiment. Because fatty acids can potentially become ^{2}H labeled via passage of ^{2}H to the acetyl group of acetyl-CoA, in addition to via NADPH, we measured acetyl group labeling (M+1) from [2,2,3,3-^{2}H]dimethyl succinate on the basis of LC-MS analysis of acetylated compounds (for example, *N*-acetyl-aspartate) relative to their unacetylated precursors (for example, aspartate), with the average labeling fraction 0.3%. Eight acetyl groups are required to produce one palmitate molecule and the probability that an acetyl-CoA

deuterated at C1 will pass that deuterium to the fatty acid chain is at most two-thirds (at least one of three C1 hydrogen atoms is lost during the fatty acyl chain extension reaction; more may be lost by H-D exchange[43]). Thus, the resulting palmitate labeling follows a binomial distribution with $n = 8$, $P = 0.002$:

$$\text{Fatty acid } {}^{2}\text{H labeling from acetyl groups} \begin{bmatrix} M_0 \\ M_1 \\ M_2 \\ \vdots \end{bmatrix} = \begin{bmatrix} 0.9841 \\ 0.0158 \\ 0.0001 \\ \vdots \end{bmatrix} \quad (13)$$

Let a_0 be the unlabeled fraction of fatty acid from NADPH, a_1 be [M+1] fraction where NADPH put one ^{2}H atom on, and so on, then $a_k = \binom{n}{k} A^k (1-A)^{n-k}$ where A is the NADP^{2}H fraction (for palmitate, $n = 14$; for additional fatty acid species, see Supplementary Fig. 7).

$$\text{Experimentally observed fatty acid labeling} = \begin{bmatrix} M_0 \times a_0 \\ M_0 \times a_1 + M_1 \times a_0 \\ M_0 \times a_2 + M_1 \times a_1 + M_2 \times a_0 \\ \vdots \end{bmatrix} \quad (14)$$

We obtained the A by least-squares fitting to a binomial function in Matlab to best match the experimentally observed fatty acid ^{2}H labeling pattern.

Metabolic flux analysis

Fluxes were computed on the basis of the network shown in Figure 4d with, in addition, cytosolic and mitochondrial aspartate and alanine transamination reactions and a protein degradation reaction that produces unlabeled amino acids in balanced amounts on the basis of their naturally occurring frequency in whole-cell protein. Measurements used to constrain the model were glucose, glutamine and oxygen uptake (with the last used to constrain total NADH production and thus TCA turning); lactate, glycerol and nonessential amino acid secretion (Supplementary Table 1); total NADPH consumption; lipid and protein synthesis rate; oxPPP flux as measured by [^{14}C]CO_2 release; ^{13}C labeling of cellular metabolites (glucose-6-phosphate, 3-phosphoglycerate, phosphoenolpyruvate, pyruvate, lactate, alanine, citrate, α-ketoglutarate, malate and aspartate) from experiments feeding [U-^{13}C]glucose or feeding [U-^{13}C]glutamine (Supplementary Fig. 3) and saponified fatty acid measurements from [U-^{13}C]glucose and [U-^{13}C]glutamine labeling experiments, which were used to compute the cytosolic labeling fractions of acetyl-CoA. When indicated, the model was also constrained with the ME1 flux as measured using ^{2}H tracers.

A cumulated isotopomer (cumomer)[44] balance model was generated using the carbon mapping network of central carbon metabolism and 13CFLUX2 software (http://www.13cflux.net)[45]. Using this model, each flux distribution simulated for both the [U-^{13}C]glucose and [U-^{13}C]glutamine conditions, and fluxes were optimized by minimizing the variance-weighted sum of squared residuals (Var-SSR) between the simulated and measured labeling fractions and uptake and secretion rates using the interior-point

algorithm[46] in Matlab. To avoid overfitting of labeling fractions that were associated (owing to unusually low random variation in the individual measurements) with an atypically small s.d., the s.d. of each individual fractional labeling measurement was floored to 0.8%, which is the mean s.d. across all such data reported herein (excluding fractional labeling <1%). As malate measurement represented the mixture of cytosolic and mitochondrial pools, a linear combination of two malate pools was fitted to the measured fractions. The non-convex optimization was solved starting from different initial flux distributions to account for the presence of local minima. Confidence intervals were estimated for a single reaction at a time by (i) starting from the best-scoring flux distribution, (ii) iteratively increasing or decreasing the flux through that reaction, (iii) optimizing all of the other fluxes, (iv) determining the increase in the objective function Var-SSR, (v) defining the upper and lower bounds of the confidence interval as the flux where Var-SSR increased by 3.84 (χ^2 cutoff for $P < 0.05$ with 1 degree of freedom)[47]. The code used for metabolic flux analysis is available from GitHub (https://github.com/PrincetonUniversity/adipocytes).

Supplementary Material

Refer to Web version on PubMed Central for supplementary material.

Acknowledgments

We thank C. Thompson and M. Birnbaum for helpful discussions. This work was supported by US National Institutes of Health grants R01CA163591 (J.D.R.), R01AI097382 (J.D.R.) and P30DK019525 (to the University of Pennsylvania Diabetes Research Center). J.F. was supported by a Howard Hughes Medical Institute fellowship. K.E.W. is supported by American Diabetes Association grant 7-12-JF-59. S.S. is supported by postdoctoral fellowship 5T32CA009140-40.

References

1. Voet, D.; Voet, J. Biochemistry. 3. Wiley; 2004.
2. Tibbetts AS, Appling DR. Compartmentalization of mammalian folate-mediated one-carbon metabolism. Annu Rev Nutr. 2010; 30:57–81. [PubMed: 20645850]
3. Wise DR, et al. Hypoxia promotes isocitrate dehydrogenase-dependent carboxylation of α-ketoglutarate to citrate to support cell growth and viability. Proc Natl Acad Sci USA. 2011; 108:19611–19616. [PubMed: 22106302]
4. WHO Working Group. Glucose-6-phosphate dehydrogenase deficiency. Bull World Health Organ. 1989; 67:601–611. [PubMed: 2633878]
5. Fan J, et al. Quantitative flux analysis reveals folate-dependent NADPH production. Nature. 2014; 510:298–302. [PubMed: 24805240]
6. Lewis CA, et al. Tracing compartmentalized NADPH metabolism in the cytosol and mitochondria of mammalian cells. Mol Cell. 2014; 55:253–263. [PubMed: 24882210]
7. Nguyen P, et al. Liver lipid metabolism. J Anim Physiol Anim Nutr (Berl). 2008; 92:272–283. [PubMed: 18477307]
8. Young JW, Shrago E, Lardy HA. Metabolic control of enzymes involved in lipogenesis and gluconeogenesis. Biochemistry. 1964; 3:1687–1692. [PubMed: 14235331]
9. Wise EM Jr, Ball EG. Malic enzyme and lipogenesis. Proc Natl Acad Sci USA. 1964; 52:1255–1263. [PubMed: 14231450]
10. Wise LS, Sul HS, Rubin CS. Coordinate regulation of the biosynthesis of ATP-citrate lyase and malic enzyme during adipocyte differentiation. Studies on 3T3-L1 cells. J Biol Chem. 1984; 259:4827–4832. [PubMed: 6201480]

11. Si Y, Yoon J, Lee K. Flux profile and modularity analysis of time-dependent metabolic changes of *de novo* adipocyte formation. Am J Physiol Endocrinol Metab. 2007; 292:E1637–E1646. [PubMed: 17284573]
12. Katz J, Rognstad R. The metabolism of tritiated glucose by rat adipose tissue. J Biol Chem. 1966; 241:3600–3610. [PubMed: 4380669]
13. Kather H, Rivera M, Brand K. Interrelationship and control of glucose metabolism and lipogenesis in isolated fat cells. Control of pentose phosphate-cycle activity by cellular requirement for reduced nicotinamide adenine dinucleotide phosphate. Biochem J. 1972; 128:1097–1102. [PubMed: 4404963]
14. Flatt JP, Ball EG. Studies on the metabolism of adipose tissue: XV. An evaluation of the major pathways of glucose catabolism as influenced by insulin and epinephrine on the metabolism of adipose. J Biol Chem. 1964; 239:675–685. [PubMed: 14154437]
15. Green H, Meuth M. An established pre-adipose cell line and its differentiation in culture. Cell. 1974; 3:127–133. [PubMed: 4426090]
16. Rosen ED, MacDougald OA. Adipocyte differentiation from the inside out. Nat Rev Mol Cell Biol. 2006; 7:885–896. [PubMed: 17139329]
17. Shreve DS, Levy HR. Kinetic mechanism of glucose-6-phosphate dehydrogenase from the lactating rat mammary gland. Implications for regulation. J Biol Chem. 1980; 255:2670–2677. [PubMed: 7358698]
18. Yang XM, MacKenzie RE. NAD-dependent methylenetetrahydrofolate dehydrogenase-methenyltetrahydrofolate cyclohydrolase is the mammalian homolog of the mitochondrial enzyme encoded by the yeast MIS1 gene. Biochemistry. 1993; 32:11118–11123. [PubMed: 8218174]
19. Ochoa S, Mehler AH, Kornberg A. Biosynthesis of dicarboxylic acids by carbon dioxide fixation; isolation and properties of an enzyme from pigeon liver catalyzing the reversible oxidative decarboxylation of 1-malic acid. J Biol Chem. 1948; 174:979–1000. [PubMed: 18871257]
20. Jitrapakdee S, et al. Structure, mechanism and regulation of pyruvate carboxylase. Biochem J. 2008; 413:369–387. [PubMed: 18613815]
21. Rutter WJ, Lardy HA. Purification and properties of pigeon liver malic enzyme. J Biol Chem. 1958; 233:374–382. [PubMed: 13563505]
22. DeBerardinis RJ, et al. Beyond aerobic glycolysis: transformed cells can engage in glutamine metabolism that exceeds the requirement for protein and nucleotide synthesis. Proc Natl Acad Sci USA. 2007; 104:19345–19350. [PubMed: 18032601]
23. Yuan Z, Hammes GG. Elementary steps in the reaction mechanism of chicken liver fatty acid synthase. pH dependence of NADPH binding and isotope rate effect for beta-ketoacyl reductase. J Biol Chem. 1984; 259:6748–6751. [PubMed: 6373765]
24. Jiang P, Du W, Mancuso A, Wellen KE, Yang X. Reciprocal regulation of p53 and malic enzymes modulates metabolism and senescence. Nature. 2013; 493:689–693. [PubMed: 23334421]
25. Si Y, Shi H, Lee K. Impact of perturbed pyruvate metabolism on adipocyte triglyceride accumulation. Metab Eng. 2009; 11:382–390. [PubMed: 19683593]
26. Kim JW, Tchernyshyov I, Semenza GL, Dang CV. HIF-1-mediated expression of pyruvate dehydrogenase kinase: a metabolic switch required for cellular adaptation to hypoxia. Cell Metab. 2006; 3:177–185. [PubMed: 16517405]
27. Lu CW, Lin SC, Chen KF, Lai YY, Tsai SJ. Induction of pyruvate dehydrogenase kinase-3 by hypoxia-inducible factor-1 promotes metabolic switch and drug resistance. J Biol Chem. 2008; 283:28106–28114. [PubMed: 18718909]
28. Hosogai N, et al. Adipose tissue hypoxia in obesity and its impact on adipocytokine dysregulation. Diabetes. 2007; 56:901–911. [PubMed: 17395738]
29. Trayhurn P. Hypoxia and adipose tissue function and dysfunction in obesity. Physiol Rev. 2013; 93:1–21. [PubMed: 23303904]
30. Mullen AR, et al. Reductive carboxylation supports growth in tumour cells with defective mitochondria. Nature. 2012; 481:385–388. [PubMed: 22101431]
31. Kamphorst JJ, Chung MK, Fan J, Rabinowitz JD. Quantitative analysis of acetyl-CoA production in hypoxic cancer cells reveals substantial contribution from acetate. Cancer Metab. 2014; 2:23. [PubMed: 25671109]

32. Price NE, Cook PF. Kinetic and chemical mechanisms of the sheep liver 6-phosphogluconate dehydrogenase. Arch Biochem Biophys. 1996; 336:215–223. [PubMed: 8954568]
33. Hermes JD, Roeske CA, O'Leary MH, Cleland WW. Use of multiple isotope effects to determine enzyme mechanisms and intrinsic isotope effects. Malic enzyme and glucose-6-phosphate dehydrogenase. Biochemistry. 1982; 21:5106–5114. [PubMed: 7138850]
34. Al-Dwairi A, Pabona JMP, Simmen RCM, Simmen FA. Cytosolic malic enzyme 1 (ME1) mediates high fat diet-induced adiposity, endocrine profile, and gastrointestinal tract proliferation-associated biomarkers in male mice. PLoS ONE. 2012; 7:e46716. [PubMed: 23056418]
35. Lee CY, Lee SM, Lewis S, Johnson FM. Identification and biochemical analysis of mouse mutants deficient in cytoplasmic malic enzyme. Biochemistry. 1980; 19:5098–5103. [PubMed: 6779864]
36. Koh HJ, et al. Cytosolic $NADP^+$-dependent isocitrate dehydrogenase plays a key role in lipid metabolism. J Biol Chem. 2004; 279:39968–39974. [PubMed: 15254034]
37. Wellen KE, et al. ATP-citrate lyase links cellular metabolism to histone acetylation. Science. 2009; 324:1076–1080. [PubMed: 19461003]
38. Boucher A, et al. Biochemical mechanism of lipid-induced impairment of glucose-stimulated insulin secretion and reversal with a malate analogue. J Biol Chem. 2004; 279:27263–27271. [PubMed: 15073188]
39. Munger J, et al. Systems-level metabolic flux profiling identifies fatty acid synthesis as a target for antiviral therapy. Nat Biotechnol. 2008; 26:1179–1186. [PubMed: 18820684]
40. Lu W, et al. Metabolomic analysis via reversed-phase ion-pairing liquid chromatography coupled to a stand alone orbitrap mass spectrometer. Anal Chem. 2010; 82:3212–3221. [PubMed: 20349993]
41. Sutterlin HA, Zhang S, Silhavy TJ. Accumulation of phosphatidic acid increases vancomycin resistance in Escherichia coli. J Bacteriol. 2014; 196:3214–3220. [PubMed: 24957626]
42. Edens WA, Urbauer JL, Cleland WW. Determination of the chemical mechanism of malic enzyme by isotope effects. Biochemistry. 1997; 36:1141–1147. [PubMed: 9033405]
43. Seyama Y, et al. Identification of sources of hydrogen atoms in fatty acids synthesized using deuterated water and stereospecifically deuterium labelled NADPH by gas chromatographic mass spectrometric analysis. Biomed Mass Spectrom. 1978; 5:357–361. [PubMed: 26434]
44. Wiechert W, Möllney M, Isermann N, Wurzel M, de Graaf AA. Bidirectional reaction steps in metabolic networks: III. Explicit solution and analysis of isotopomer labeling systems. Biotechnol Bioeng. 1999; 66:69–85. [PubMed: 10567066]
45. Weitzel M, et al. ^{13}CFLUX2—high-performance software suite for ^{13}C metabolic flux analysis. Bioinformatics. 2013; 29:143–145. [PubMed: 23110970]
46. Waltz RA, Morales JL, Nocedal J, Orban D. An interior algorithm for nonlinear optimization that combines line search and trust region steps. Math Program. 2006; 107:391–408.
47. Antoniewicz MR, Kelleher JK, Stephanopoulos G. Determination of confidence intervals of metabolic fluxes estimated from stable isotope measurements. Metab Eng. 2006; 8:324–337. [PubMed: 16631402]

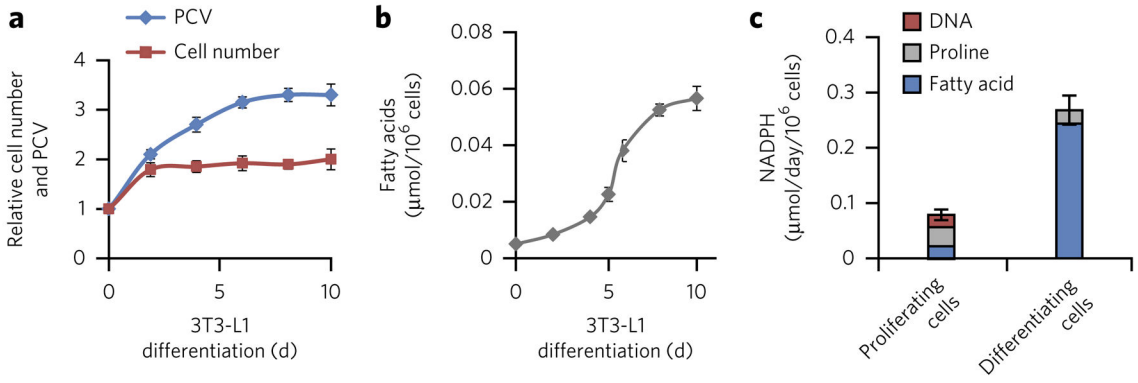

Figure 1. NADPH consumption during adipogenesis

(**a**) Changes in cell number and packed cell volume (PCV) in normoxic 3T3-L1 cells after initiation of differentiation; values are relative to day 0. (**b**) Total saponified fatty acids from cells in **a**. (**c**) NADPH biosynthetic consumption flux in proliferating and differentiating (day 5) 3T3-L1 cells. Data are mean ± s.d., $n = 3$ independent culture dishes analyzed in parallel (similar results were obtained on two independent occasions).

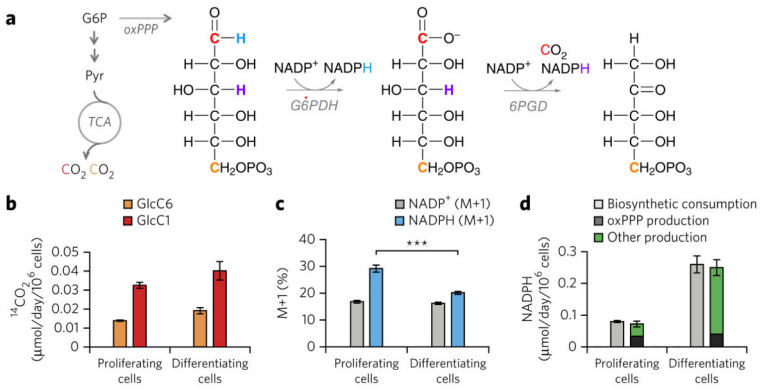

Figure 2. NADPH production by the oxPPP

(**a**) Schematic of the oxPPP. 6PGD, 6-phosphogluconate dehydrogenase. (**b**) $^{14}CO_2$ release from [1-^{14}C]glucose and [6-^{14}C]glucose. The rate of $^{14}CO_2$ release from [1-^{14}C]glucose minus that from [6-^{14}C]glucose reflects the oxPPP flux. Data are from normoxic proliferating or differentiating (day 5) 3T3-L1 cells. (**c**) $NADP^+$ and NADPH ^{2}H labeling in proliferating and differentiating cells fed [1-^{2}H]glucose for 2 h. ***$P < 0.001$, *t*-test. (**d**) Comparison of NADPH production with biosynthetic NADPH consumption. Total NADPH consumption was calculated from absolute oxPPP flux (**b**) divided by $NADP^2H$ fraction measured by NADPH labeling in **c**. Data are mean ± s.d., $n = 3$ independent culture dishes analyzed in parallel (similar results were obtained on two independent occasions).

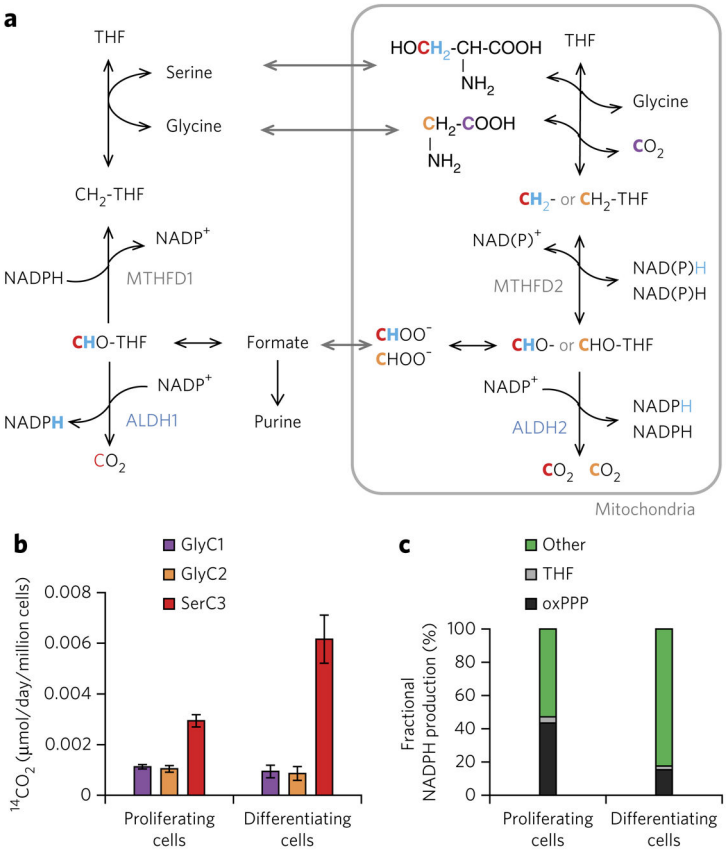

Figure 3. NADPH production by folate metabolism

(**a**) Folate pathway schematic. (**b**) $^{14}CO_2$ release from normoxic proliferating or differentiating (day 5) 3T3-L1 cells fed [1-^{14}C]glycine (GlyC1), [2-^{14}C]glycine (GlyC2) or [3-^{14}C]serine (SerC3). (**c**) Fractional NADPH contribution of the oxPPP, the folate pathway (THF) and other sources in proliferating and differentiating cells as in **b**. The estimate of NADPH produced by folate metabolism assumes that MTHFD2 produces NADH. Data are mean ± s.d., $n = 3$ independent culture dishes analyzed in parallel (similar results were obtained on two independent occasions).

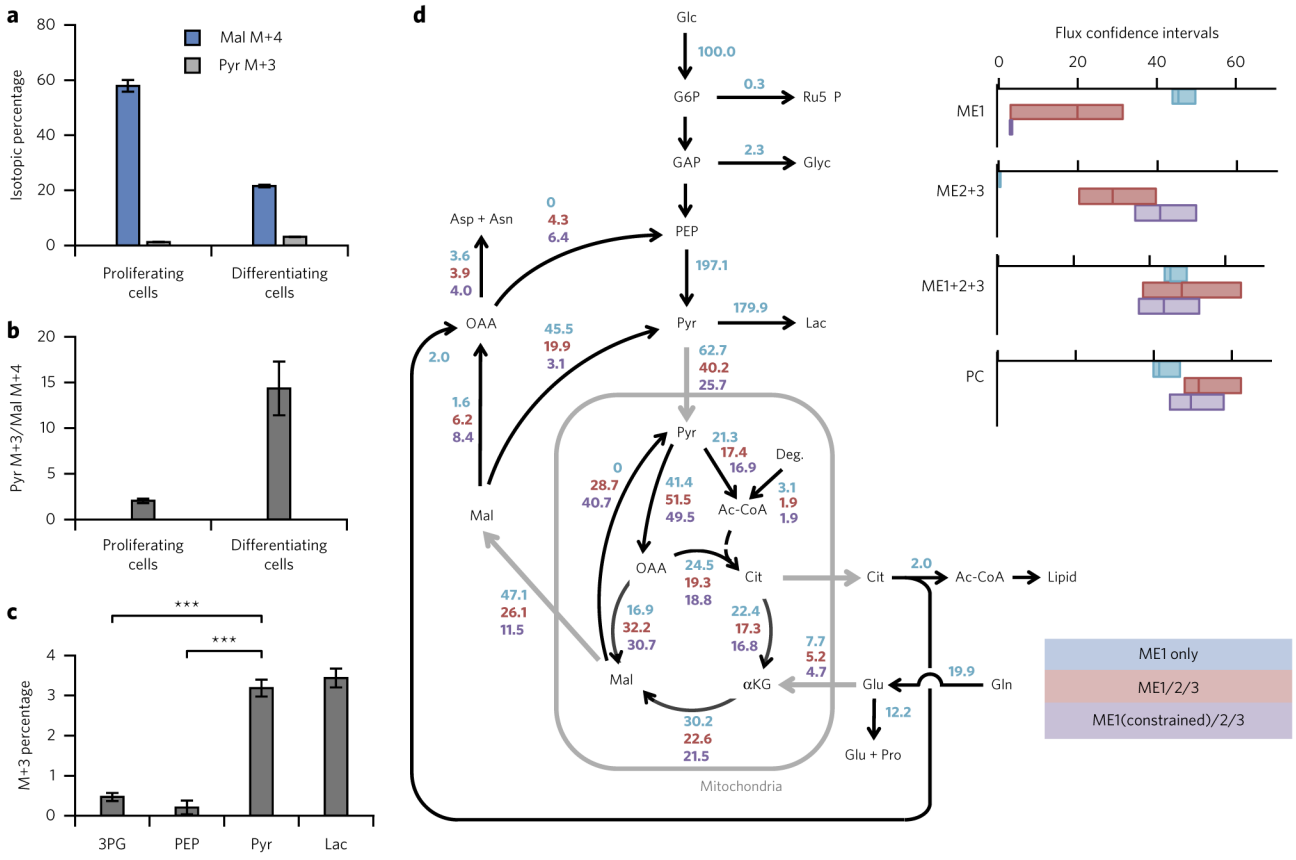

Figure 4. Carbon flux through malic enzyme

(**a**,**b**) Production of malate M+4 and pyruvate M+3 from [U-^{13}C]glutamine (12 h labeling) (**a**) and abundance of pyruvate M+3 relative to malate M+4 (**b**) in normoxic proliferating or differentiating (day 5) 3T3-L1 cells. (**c**) Associated production in differentiating 3T3-L1 adipocytes of M+3–labeled 3-phosphoglycerate (3PG), PEP, pyruvate (pyr) and lactate (lac). (**d**) Central carbon metabolic flux in differentiating 3T3-L1 adipocytes based on metabolic flux analysis informed by nutrient uptake, waste excretion and biomass production flux, as well as LC-MS analysis of intracellular metabolite labeling in cells fed [U-^{13}C]glucose or [U-^{13}C]glutamine. Shown are relative flux values (normalized to glucose uptake) from the best fit flux sets for a simplified network with ME1 only (blue), a network with inclusion of mitochondrial enzymes ME2 or ME3 (ME1/2/3, red) and constraint of the ME1 flux using ^{2}H-labeling data (ME1(constrained)/2/3, purple numbers). Flux values <10% different from the ME1 only values are not shown. Inset, confidence intervals for malic enzyme and pyruvate carboxylase flux. For complete flux distributions and confidence intervals, see Supplementary Table 1. GAP, glyceraldehyde-3-phosphate; glyc, glycerol; OAA, oxaloacetate; αKG, α-ketoglutarate; cit, citrate; Ac-CoA, acetyl-CoA. ***$P < 0.001$, t-test; data are mean ± s.d., $n = 3$ (**a**–**c**) independent culture dishes analyzed in parallel (similar results were obtained on three independent occasions).

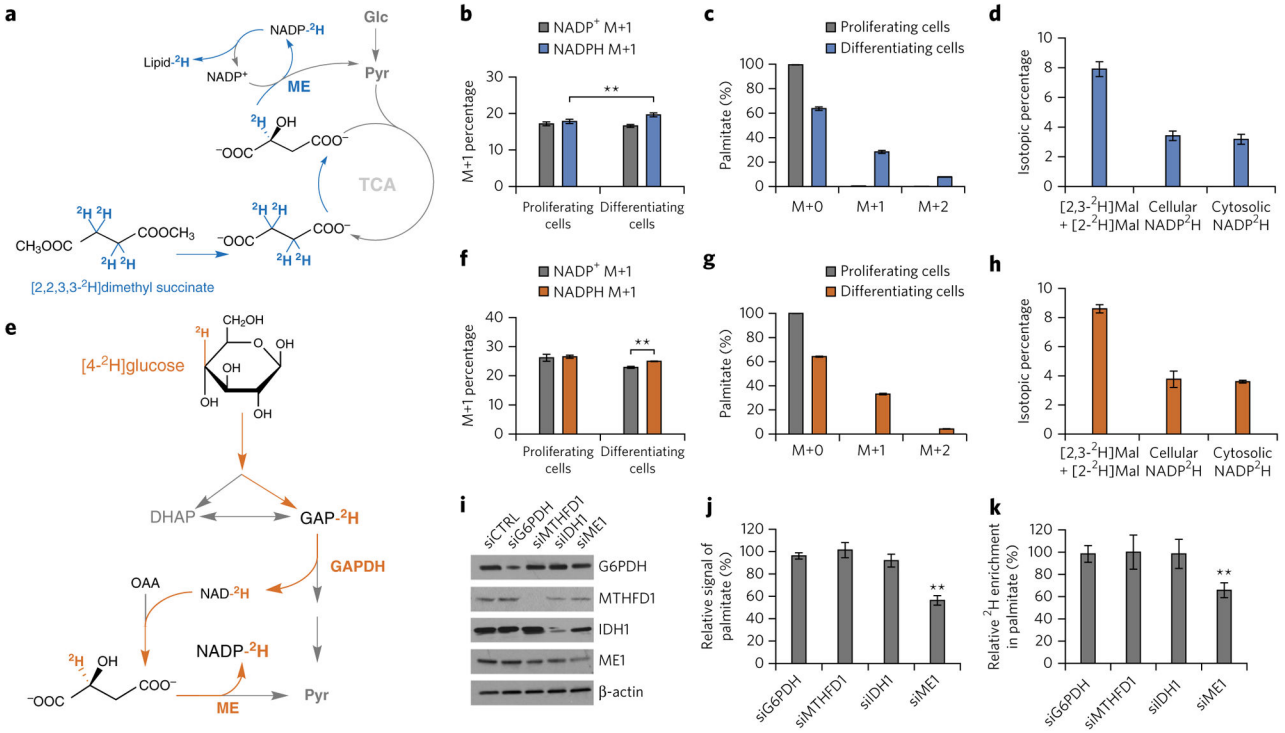

Figure 5. Tracing hydride flux through malic enzyme

(**a**) Schematic of [2,2,3,3-^{2}H]dimethyl succinate metabolism in normoxic proliferating or differentiating (day 5) 3T3-L1 cells. (**b**) $NADP^+$ and NADPH ^{2}H labeling in proliferating or differentiating cells fed [2,2,3,3-^{2}H]dimethyl succinate for 24 h. (**c**) Palmitate ^{2}H labeling in cells fed [2,2,3,3-^{2}H]dimethyl succinate for 5 d. (**d**) Extent of ^{2}H labeling of the redox-active hydrogen of malate (mal), whole-cell NADPH and cytosolic NADPH (inferred from fatty acid labeling) in differentiating 3T3-L1 adipocytes fed [2,2,3,3-^{2}H]dimethyl succinate (labeling duration 24 h except for the fatty acids, which was 5 d). (**e**) Schematic of [4-^{2}H]glucose metabolism. (**f**) $NADP^+$ and NADPH ^{2}H labeling in cells fed [4-^{2}H]glucose for 24 h. (**g**) Palmitate ^{2}H labeling in cells fed [4-^{2}H]glucose for 5 d. (**h**) Extent of ^{2}H labeling of the redox-active hydrogen of malate, whole-cell NADPH and cytosolic NADPH (inferred from fatty acid labeling) in differentiating 3T3-L1 adipocytes fed [4-^{2}H]glucose. (**i**) Immunoblot analysis of siRNA-mediated knockdown (si-) of G6PDH, MTHFD1, IDH1 and ME1 in differentiating 3T3-L1 adipocytes (full gel images are shown in Supplementary Fig. 13). siCTRL, pool of four siRNAs tested for minimal targeting of mouse genes. (**j**) Impact of knockdown of NADPH-producing enzymes on total cellular palmitate abundance (free + saponified from lipids). (**k**) Impact NADPH-producing enzyme knockdown on palmitate ^{2}H labeling from [2,2,3,3-^{2}H]dimethyl succinate. Results are normalized to siCTRL-treated cells. $^{**}P < 0.01$, *t*-test; data are mean ± s.d., $n = 3$ independent culture dishes analyzed in parallel (similar results were obtained on three independent occasions).

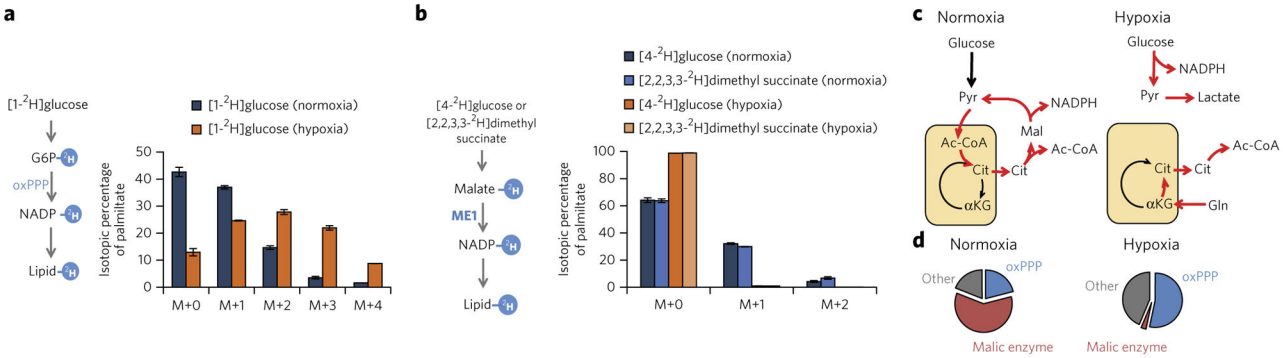

Figure 6. Hypoxia increases adipocyte NADPH production by the oxPPP and blocks that by malic enzyme

(**a**) Labeling of palmitate in 3T3-L1 adipocytes fed [1-^{2}H]glucose to trace cytosolic NADPH production by the oxPPP in the presence of ambient oxygen (normoxia) or 1% oxygen (hypoxia). (**b**) Labeling of palmitate in 3T3-L1 adipocytes fed [4-^{2}H]glucose or [2,2,3,3-^{2}H]dimethyl succinate to trace cytosolic NADPH production by malic enzyme. Cells were cultured throughout the 5-d differentiation period in the presence of tracer and either ambient oxygen (normoxia) or 1% oxygen (hypoxia). (**c**) Summary of metabolic activity in differentiating normoxic or hypoxic adipocytes showing disruption of the citrate-pyruvate cycle in hypoxia and its replacement by reductive carboxylation, with a concomitant shift away from NADPH production by malic enzyme. αKG, α-ketoglutarate; cit, citrate; Ac-CoA, acetyl-CoA; mal, malate; pyr, pyruvate. (**d**) Quantitative comparison of NADPH production routes in differentiating adipocytes in conditions of normoxia and hypoxia. Data are mean ± s.d., $n = 3$ independent culture dishes analyzed in parallel (similar results were obtained on two independent occasions).